Analytical solution to predicting gaseous mass flow rates of microchannels in a wide range of Knudsen numbers

Qifeng Lv,* Xiaoli Liu, Enzhi Wang, and Sijing Wang
State Key Laboratory of Hydroscience and Engineering, Tsinghua University, Beijing 100084, China
(Received 11 December 2012; revised manuscript received 10 June 2013; published 15 July 2013)

To predict the gaseous mass flow rate of microchannels, conventional analytical solutions based on the Navier-Stokes equation or volume diffusion hydrodynamics (bivelocity hydrodynamics) associated with first-order or second-order slip boundary condition are not very successful, especially in high-Knudsen-number flow. An analytical solution which agrees with experimental data to a Knudsen number of 50 is presented in this paper. To achieve this goal, a concept of effective volume diffusion is defined. Then, with a general slip boundary condition, the gaseous mass flow rate of microchannel is derived by solving the momentum equation of this effective volume diffusion hydrodynamics. Compared with six other analytical solutions and one group of numerical solutions of the linearized Boltzmann equation, this solution is validated by three groups of experimental data. The results not only illustrate an improvement of this solution compared with other analytical solutions but also show the importance of the effective volume diffusion hydrodynamics for compressible microfluids.

DOI: 10.1103/PhysRevE.88.013007 PACS number(s): 47.61.−k, 47.40.−x, 47.45.−n

I. INTRODUCTION

Analytical solutions to predicting the gaseous mass flow rate of microchannels (see Fig. 1) are of great interest in many fields. Since Maxwell's first-order slip boundary condition [1] was introduced, the Navier-Stokes equation can give a satisfactory solution in the continuum and slip flow regime (Kn $<$ 0.1, where Kn is the Knudsen number) [2]. For higher-Knudsen-number flow, many analytical works have been carried out, but they are much less successful than their counterpart, numerical solutions, e.g., direct simulation Monte Carlo [3] and linearized Boltzmann equation [4].

Analytical solutions to this problem are always only suitable at a lower Knudsen number, below unity [5–7]. This is because the terms which are cut off in the Taylor series expansion for the fluid's boundary velocity will become significant when the Knudsen number increases above 1. Therefore the inaccuracy will become larger and larger along with the rising Knudsen number. Even with the use of a higher order slip boundary condition, this improves little [8–10]. What we really need is a special slip boundary condition which can compensate the cutoff terms when the Knudsen number increases above 1.

Such a different kind of slip boundary condition, called the general slip boundary condition [11], was proposed by Beskok and Karniadakis. For this problem, Karniadakis and Beskok [12] derived a mass flow rate expression by solving the Navier-Stokes equation associated with their general slip boundary condition. Their comparison with direct simulation Monte Carlo data agrees well up to a Knudsen number of 5. Moreover, the Knudsen minimum is also successfully captured by their model.

Besides the research on boundary conditions, diffusion theory is also considered widely. Veltzke and Thöming [6] added a diffusion term based on Fick's law to the Navier-Stokes solution with no slip boundary condition. Their model can agree with experimental data up to a Knudsen number of 0.4.

With a first-order slip boundary condition, Graur *et al.* [5] derived an analytical model for this problem from quasi-gas-dynamics equations. The realm of their model's applicability is also within the Knudsen number of 0.4.

By introducing a volume velocity, Brenner's volume diffusion hydrodynamics [13] sheds a fresh light on this problem. On the basis of this theory and a first-order slip boundary condition, an analytical solution was derived by Dadzie and Brenner [14]. Their solution agreed with Ewart *et al.*'s experimental data [15] to a Knudsen number of 5.

In this paper, an analytical solution is derived in Sec. II, which agrees satisfactorily with experimental data [15] to a Knudsen number of 50. To achieve this goal, we define a concept of effective volume diffusion in Sec. II B based on Brenner's volume diffusion hydrodynamics (Sec. II A). Section II C introduces Beskok and Karniadakis' general slip boundary condition [11,12]. Combining the effective volume diffusion and the general slip boundary condition, we derive the mass flow rate expression in Sec. II D. To validate our model, we compare our solution, other solutions, and Ewart *et al.*'s experimental data in Sec. III. Moreover, the present model is analyzed in Sec. IV. Finally, Sec. V presents a brief conclusion.

II. ANALYTICAL SOLUTION

A. Volume diffusion

Volume diffusion hydrodynamics was proposed for compressible fluids [16], which is characterized by two velocities (i.e., the volume velocity and mass velocity, which represent the velocities of the volume center and mass center, respectively). The relationship between them can be expressed as [13,17]

$$\mathbf{U_v} = \mathbf{U_m} + \mathbf{J_v}, \tag{1}$$

in which $\mathbf{U_v}$ denotes the volume velocity, which can be measured with a small macroscopic solid particle suspended in the compressible fluid, and $\mathbf{U_m}$ denotes the mass velocity appearing in the continuity equation, which can be measured

*keephong@126.com

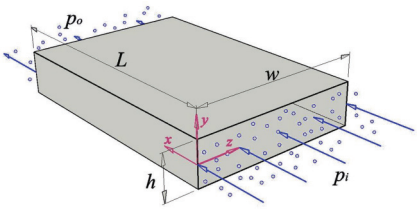

FIG. 1. (Color online) Schematic of rarefied gas flow in a microchannel. L is the channel length, h is its height, w is its width, p_i is the inlet pressure, and p_o is the outlet pressure. Here we consider only the infinitely long channel where $L, w \gg h$. Circles represent rarefied gas, darker (blue) arrows represent the flow direction, and lighter (red) arrows (labeled x, y, and z) are the coordinate axes.

with a molecular-tagging dye (see Fig. 2). The volume diffusion flux $\mathbf{J_v}$ is given by [13]

$$\mathbf{J_v} = \kappa_m \nabla \ln \rho = \frac{k}{c_p \rho} \nabla \ln \rho, \tag{2}$$

where κ_m is the diffusion coefficient, ρ is the density, k is the Fourier thermal conductivity, and c_p is the specific heat at constant pressure. On the basis of this assumption, the continuity and momentum equations can be written as [13]

$$\frac{\partial \rho}{\partial t} + \nabla \cdot (\rho \mathbf{U_m}) = 0 \tag{3}$$

and

$$\frac{\partial (\rho \mathbf{U_m})}{\partial t} + \nabla \cdot (\rho \mathbf{U_m} \mathbf{U_m}) = \mu \nabla^2 \mathbf{U_v} + \frac{1}{3} \mu \nabla (\nabla \cdot \mathbf{U_v}) - \nabla p, \tag{4}$$

respectively, and where p is the fluid pressure and μ is the shear viscosity. For incompressible fluids, $\mathbf{J_v} = 0$, these governing equations will be reduced to Navier-Stokes equations.

B. Effective volume diffusion

For the compressible microfluid which is confined by micro solid walls, its molecular mean free path λ should not be the same as that without boundary confinement [10,18]. Therefore, an effective mean free path λ_e must exist in this

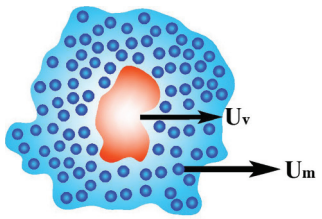

FIG. 2. (Color online) Schematic of the mass velocity $\mathbf{U_m}$ and volume velocity $\mathbf{U_v}$ in volume diffusion hydrodynamics. The (light-blue) background represents compressible fluid, in which the darker (dark-blue) circles represent fluid molecules. The (red) irregularshaped area in the middle is a suspending particle (we term it the volume diffusion particle) in the fluid. In reality, the volume diffusion particle is much larger than the molecules. Both $\mathbf{U_m}$ and $\mathbf{U_v}$ are macroscopic concepts ($\mathbf{U_m}$ is not the molecular thermal velocity and $\mathbf{U_v}$ does not represent the velocity of the Brownian particle, which is indeed smaller than the volume diffusion particle).

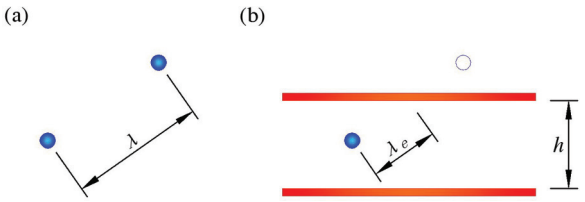

FIG. 3. (Color online) Schematic of the micro boundary effect of microfluids. Filled (blue) circles represent fluid molecules, and thick horizontal (red) bars represent the microdevice's solid wall. λ is the molecular mean free path, λ_e is the effective mean free path, and h is the distance between the solid walls. Indeed, λ_e functionally depends on the Knudsen number, Kn. Therefore, influenced by the effective mean free path, the microfluid's transport coeficients, i.e., diffusion, viscosity, and thermal conductivity, must be functions of the Knudsen number. (a) Macrofluid; (b) microfluid.

situation (see Fig. 3). On the basis of this fact, the three basic transport coefficients (i.e., diffusion, viscosity, and thermal conductivity) which are affected by the molecular mean free path should also have an effective value for the compressible microfluid (e.g., high-Knudsen-number flow).

From this point, the volume diffusion flux $\mathbf{J_v}$, which is a function of the thermal conductivity k, should also consider the micro boundary effect when the Knudsen number is high. Therefore, we define the effective volume diffusion flux as

$$\mathbf{J_{ve}} = \frac{k_e}{c_p \rho} \nabla \ln \rho, \tag{5}$$

where k_e is the effective thermal conductivity, which should be a function of the Knudsen number for the microfluid. Because the Prandtl number $\mathrm{Pr} = \mu c_p / k$, we have $k_e = \mu_e c_p / \mathrm{Pr}$, in which μ_e is the effective viscosity. Substituting k_e into Eq. (5), we have

$$\mathbf{J_{ve}} = \frac{\mu_e}{\mathrm{Pr} \rho} \nabla \ln \rho. \tag{6}$$

By rarefaction coefficient theory [11,12], the effective viscosity can be written as

$$\mu_e = \mu \frac{1}{1 + a\mathrm{Kn}}, \tag{7}$$

where a is a rarefaction coefficient which is an empirical parameter. For simplicity, a is used as a constant in our deduction. This was also suggested by Michalis *et al.* in Ref. [19].

Substituting Eq. (7) into Eq. (6), we have the final expression for the effective volume diffusion flux:

$$\mathbf{J_{ve}} = \frac{\mu}{(1 + a\mathrm{Kn})\mathrm{Pr} \rho} \nabla \ln \rho. \tag{8}$$

Similarly, by introducing Eq. (7), the momentum equation for this effective volume diffusion hydrodynamics can be written as

$$\frac{\partial (\rho \mathbf{U_m})}{\partial t} + \nabla \cdot (\rho \mathbf{U_m} \mathbf{U_m}) = \mu_e \nabla^2 \mathbf{U_v} + \frac{1}{3} \mu_e \nabla (\nabla \cdot \mathbf{U_v}) - \nabla p. \tag{9}$$

C. General slip boundary condition

On the basis of kinetic theory, Maxwell proposed a first-order slip boundary condition [1] to accelerate the Navier-Stokes velocity for high-Knudsen-number flow. However, when the Knudsen number increases above 1, this kind of slip boundary condition (including second and higher orders) [8,9,14] will bring an unrealistic velocity (too slow or too fast). This is because the cutoff terms in the Taylor series expansion of the boundary velocity will becomes significant (i.e., the cutoff terms should not be cut off). To be out of this dilemma, Beskok and Karniadakis' general slip boundary condition [11,12] is helpful. The reason is that this general slip boundary condition can compensate the cutoff terms when the Knudsen number increases above 1. Therefore, we use this boundary condition in our deduction and present an adjusted form as below:

$$u_{vx}(x,\pm h/2) = \mp K_s \frac{\lambda h}{h+b\lambda}\left(\frac{\partial u_{vx}}{\partial y}\right)_{y=h/2}, \tag{10}$$

in which

$$K_s = \frac{2-\alpha}{\alpha} \tag{11}$$

is the Maxwell's slip coefficient, α is the momentum accommodation coefficient, and b is the general slip coefficient, which is an empirical parameter. When $b=0$, Eq. (10) will be reduced to Maxwell's first-order slip boundary condition [5,20].

D. Mass flow rate

For this problem, rarefied gas flowing in a microchannel (see Fig. 1) whose length is L along the direction of the coordinate x and whose height is h along the direction of the coordinate y, Eq. (1) associated with Eq. (6) can be rewritten as (the width $w \gg h$, so the flow can be seen as two-dimensional)

$$u_{vx} = u_{mx} + \frac{\mu_e}{\Pr\rho}\nabla\ln\rho, \tag{12a}$$

$$u_{vy} = u_{my}. \tag{12b}$$

The momentum equation, Eq. (9), can be reduced as

$$\mu_e \frac{\partial^2 u_{vx}}{\partial y^2} = \frac{dp}{dx}. \tag{13}$$

The solution of Eq. (13) satisfying the general slip boundary condition, (10), is

$$u_{vx} = \frac{1}{8\mu_e}\frac{dp}{dx}\left(4y^2 - h^2 - 4K_s h^2\frac{\mathrm{Kn}}{1+b\mathrm{Kn}}\right), \tag{14}$$

where $\mathrm{Kn} = \lambda/h$. Substituting Eq. (14) into (12a), u_{mx} can be obtained as below:

$$u_{mx} = \frac{1}{8\mu_e}\frac{dp}{dx}\left(4y^2 - h^2 - 4K_s h^2\frac{\mathrm{Kn}}{1+b\mathrm{Kn}}\right) - \frac{\mu_e}{\Pr\rho}\frac{d\ln\rho}{dx}. \tag{15}$$

Integrating Eq. (15) along y and taking the microchannel's width w into account yields

$$\dot{Q} = \int_{-h/2}^{h/2} w u_{mx} dy = -\frac{wh^3}{12\mu_e}\frac{dp}{dx}\left(1 + \frac{6K_s\mathrm{Kn}}{1+b\mathrm{Kn}}\right) - \frac{\mu_e wh}{\Pr\rho}\frac{d\ln\rho}{dx}, \tag{16}$$

where $\dot{Q}$ is the volume flow rate. Substituting Eq. (7) into Eq. (16), we have

$$\dot{Q} = -\frac{wh^3}{12\mu}\frac{dp}{dx}(1+a\mathrm{Kn})\left(1 + \frac{6K_s\mathrm{Kn}}{1+b\mathrm{Kn}}\right) - \frac{wh}{\Pr\rho}\frac{\mu}{1+a\mathrm{Kn}}\frac{d\ln\rho}{dx}. \tag{17}$$

Then the mass flow rate of the microchannel can be obtained by

$$\dot{M} = \frac{\int \rho\dot{Q}dx}{L}, \tag{18}$$

in which $\rho = p/RT$. R is the specific gas constant, and T is the temperature. The Knudsen number can be expressed as a function of the local pressure by $\mathrm{Kn} = \mathrm{Kn}_o p_o/p$, where the subscript o refers to the outlet condition (i inlet). Substituting Eq. (17), ρ, and Kn into (18), $\dot{M}$ can be integrated as

$$\dot{M} = \frac{wh^3 p_o^2}{24L\mu RT}\left[(P^2-1) + (12K_s + 2a)(P-1)\mathrm{Kn}_o + 12K_s(a-b)\mathrm{Kn}_o^2\ln\frac{P+b\mathrm{Kn}_o}{1+b\mathrm{Kn}_o} + \frac{48}{\Pr\pi}\mathrm{Kn}_o^2\ln\frac{P+a\mathrm{Kn}_o}{1+a\mathrm{Kn}_o}\right], \tag{19}$$

where $P = p_i/p_o$ is the inlet-to-outlet pressure ratio.

In Eq. (19), the first term is the solution of the Navier-Stokes equation with no slip at the boundary, namely,

$$\dot{M} = \frac{wh^3 p_o^2}{24L\mu RT}(P^2-1). \tag{20}$$

When $a=0$, $b=0$, Eq. (19) will be reduced to Dadzie and Brenner's solution [14]. After taking the geometry effect (L/w) into the volume diffusion coefficient κ_m, their final solution is

$$\dot{M} = \frac{wh^3 p_o^2}{24L\mu RT}\left[(P^2-1) + 12K_s\mathrm{Kn}_o(P-1) + \frac{48w}{\Pr L\pi}\mathrm{Kn}_o^2\ln P\right]. \tag{21}$$

By a similar deduction process, we can also derive another general mass flow rate expression from the Navier-Stokes equation associated with the second-order slip boundary condition, which can be written as

$$\dot{M} = \frac{wh^3 p_o^2}{24L\mu RT}\left[(P^2-1) + 12K_s c_1\mathrm{Kn}_o(P-1) + 24K_s c_2\mathrm{Kn}_o^2\ln P\right], \tag{22}$$

where c_1 and c_2 are the slip coefficients. When $c_1 = 1$ and $c_2 = 0$, $\dot{M}$ will be reduced to the solution for Maxwell's first-order slip boundary condition [1]. Deissler employed $c_1 = 1$ and $c_2 = 1.6875$ for the second-order slip coefficients, and Cercignani used $c_1 = 1.1466$ and $c_2 = 0.9756$, whereas Sreekanth used $c_1 = 1.1466$ and $c_2 = 0.14$ [21].

TABLE I. Parameter values for the comparison and analysis.

Parameter	Value
L	429 mm
h	9.39×10^{-6} m
w	9.38×10^{-6} m
a	0.85
b	2.95
T	296 K
μ	19.67×10^{-6} Pa · s
R	2078.5 J/(kg · K)
Pr	2/3
P	
Group 1	5
Group 2	4
Group 3	3
α	
Group 1	0.900
Group 2	0.903
Group 3	0.938
K_s	
Group 1	1.222
Group 2	1.215
Group 3	1.132

III. COMPARISON

The comparisons are among the present analytical solution [Eq. (19)], other analytical solutions [i.e., Eqs. (20)–(22)], Ohwada *et al.*'s numerical solution of the linearized Boltzmann equation [4], and the experimental data of Ewart *et al.* [15]. The parameter values used in our comparisons are presented in Table I, in which a, b, and $K_s(\alpha)$ are empirical parameters, and the others are physical parameters for Ewart *et al.*'s experiments. The values of $K_s(\alpha)$ were chosen by Ewart *et al.* [15]. We chose the values of a and b. A detailed discussion of these three empirical parameters is presented in Sec. IV.

Ohwada *et al.*'s numerical solution of the linearized Boltzmann equation [4] requires that the pressure gradient P is small and the boundary condition is fully diffuse reflection ($K_s = 1$). These assumptions are closer to the situation for the third group of experimental data.

All the figures are plotted in the form of a dimensionless mass flow rate G_m versus the mean Knudsen number expressed as [12,22]

$$\mathrm{Kn}_m = \frac{\mu}{h\frac{p_i+p_o}{2}}\sqrt{\frac{\pi RT}{2}}. \tag{23}$$

Then we have

$$\mathrm{Kn}_o = \frac{P+1}{2}\mathrm{Kn}_m. \tag{24}$$

With the use of Eq. (24), the mass flow rate expressions can be rearranged as a function of Kn_m. The dimensionless mass flow rate G_m is calculated by

$$G_m = \dot{M}\left[\frac{wh^2}{L\sqrt{2RT}}(p_i - p_o)\right]^{-1}. \tag{25}$$

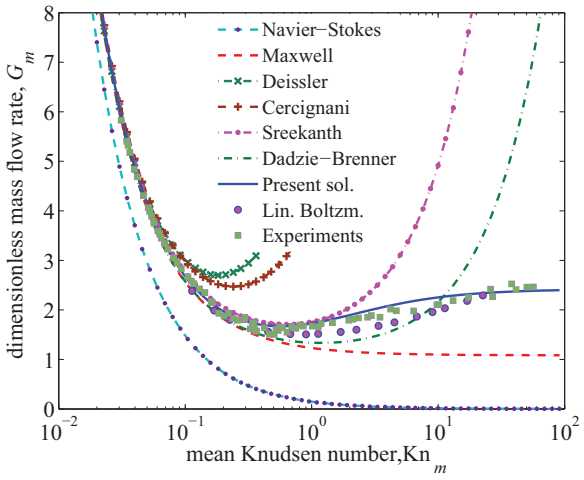

FIG. 4. (Color online) Comparison among the present analytical solution, other analytical solutions, the numerical solution of the linearized Boltzmann equation [4], and the experimental data (group 1, $P = 5$) [15]. Kn_m and G_m are calculated by Eqs. (23) and (25), respectively. "Navier-Stokes," "Dadzie-Brenner," and "present sol." represent Eqs. (19)–(21), respectively. "Maxwell," "Deissler," "Cercignani," and "Sreekanth" represent, respectively, Eq. (22) with slip coefficients $c_1 = 1$ and $c_2 = 0$, $c_1 = 1$ and $c_2 = 1.6875$, $c_1 = 1.1466$ and $c_2 = 0.9756$, and $c_1 = 1.1466$ and $c_2 = 0.14$. "Lin. Boltzm." represents Ohwada *et al.*'s numerical solution of the linearized Boltzmann equation [4].

Figures 4, 5, and 6 are the comparison results. Clearly, the present solution agrees satisfactorily with the experimental data to a Knudsen number of 50. In the slip flow regime ($0.01 < \mathrm{Kn}_m < 0.1$), all solutions agree well with the experimental data except the Navier-Stokes solution, which diverges significantly.

In the earlier transitional flow regime ($0.1 < \mathrm{Kn}_m < 1$), Maxwell's, Deissler's, and Cercignani's solutions began to break down, whereas Sreekanth's solution can reach a Knudsen number of 1.5. These four solutions are based on the

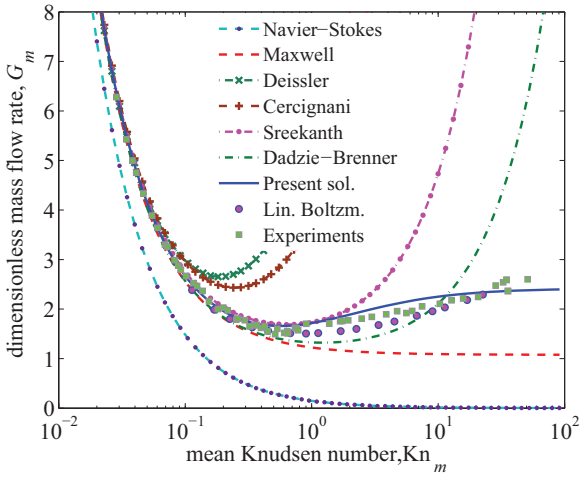

FIG. 5. (Color online) Comparison among the present analytical solution, other analytical solutions, the numerical solution of the linearized Boltzmann equation [4], and the experimental data (group 2, $P = 4$) [15].

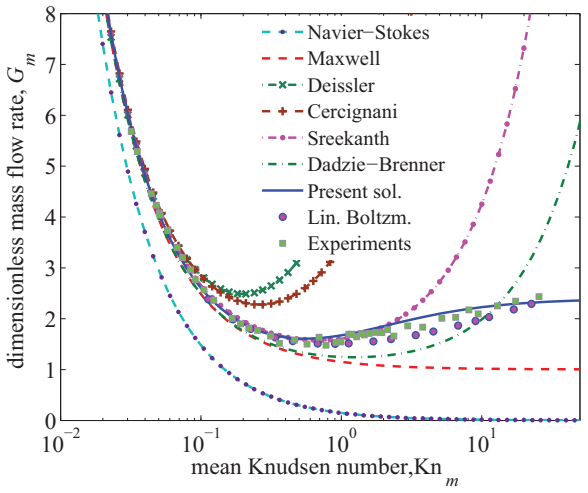

FIG. 6. (Color online) Comparison among the present analytical solution, other analytical solutions, the numerical solution of the linearized Boltzmann equation [4], and the experimental data (group 3, $P = 3$) [15].

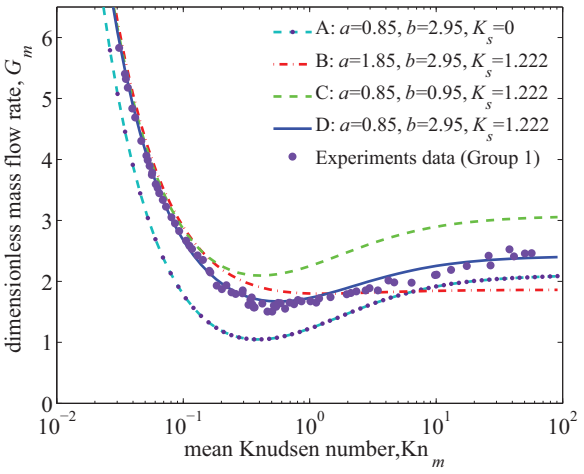

FIG. 7. (Color online) Role of empirical parameters in the present model. A brief conclusion can be made: (i) K_s accelerates the Navier-Stokes velocity in lower-Knudsen-number flow; and (ii) a and b capture the Knudsen minimum and control the velocity when the Knudsen number is high.

Navier-Stokes equation. Dadzie-Brenner's solution and present solution are based on volume diffusion hydrodynamics, which, as well as the numerical solution of the linearized Boltzmann equation, agree well with the experimental data when $\mathrm{Kn}_m < 0.7$.

In the later transitional flow regime ($1 < \mathrm{Kn}_m < 10$), which is the most difficult regime to predict, the mass flow rate of the numerical solution (linearized Boltzmann equation) is a little bit slower than that of the experiments, and the present solution is slightly faster, but the results are still satisfactory within a tolerable deviation. Beginning from the transitional flow regime, Dadzie-Brenner's solution shows a sharp rise, which also appears in Deissler's, Cercignani's, and Sreekanth's solution. This is because the micro boundary effect (Fig. 3) was not considered. In the present model, because the effective volume diffusion is introduced, the mass flow rate climbs moderately in the transitional flow regime.

In the free molecular flow regime ($\mathrm{Kn}_m > 10$), around the mean Knudsen number of 50, the present solution approaches a constant value, but logarithmic growth in the Knudsen number was concluded by the asymptotic analysis of the Boltzmann equtation [23,24] in the highly rarefied gas flow when $\mathrm{Kn} \to \infty$. Therefore, the Knudsen number of 50 is the limit of the present analytical solution. The reason for this limit is that constant empirical parameters are used in order to derive a simple and clear analytical solution, but the present models are rigorous and contain all the physics that are needed for this problem. Compared with other analytical solutions, clearly the present solution shows a significant improvement for predicting rarefied gas flow.

IV. ANALYSIS

Because the effective volume diffusion flux and the general slip boundary condition are based on kinetic theory, the present model is a hybrid of the continuum and kinetic models. Thus, the present solution can predict the gaseous mass flow rate over a wide range of Knudsen numbers.

Three empirical parameters appear in the present model. Their physical role is connecting kinetic theory with continuum theory. When $a = b = K_s = 0$, the present model will be reduced to the Navier-Stokes continuum model. A visual analysis of these three empirical parameters is illustrated in Fig. 7. Comparing line A with the other lines in Fig. 7, we find that K_s plays an important role in accelerating the Navier-Stokes velocity when the flow is in a lower Knudsen number. The difference between line C and line D means that b is mainly used to capture the Knudsen minimum. For a, comparing lines B and D, we find that it is useful to control the velocity in a high-Knudsen-number flow.

To understand the present model more thoroughly, we plot the mass velocity and volume velocity profiles in Fig. 8, which also contains the numerical solution of the linearized Boltzmann equation [4]. In Fig. 8, the dimensionless mean mass velocity U_{mx} and dimensionless mean volume velocity U_{vx} are calculated by

$$U_{mx} = \frac{\int \rho u_{mx} dx}{L} \left[\frac{h}{L\sqrt{2RT}} (p_i - p_o) \right]^{-1} \tag{26}$$

and

$$U_{vx} = \frac{\int \rho u_{vx} dx}{L} \left[\frac{h}{L\sqrt{2RT}} (p_i - p_o) \right]^{-1}, \tag{27}$$

respectively. Because the linearized Boltzmann solution requires the diffuse reflection condition, we use $K_s = 1$ in Fig. 8. The other parameter values are the same as those in Sec. III.

Clearly, besides the satisfactory agreement with the numerical solution of the linearized Boltzmann equation, the present model bridges the incompressible and compressible flow (see Fig. 8). In Fig. 8, the mass velocity and the volume velocity are the same in the incompressible flow ($\mathrm{Kn} \ll 1$). Both the mass velocity and the volume velocity decrease along with the increasing Knudsen number before the Knudsen minimum. Past the Knudsen minimum, the mass velocity bounces

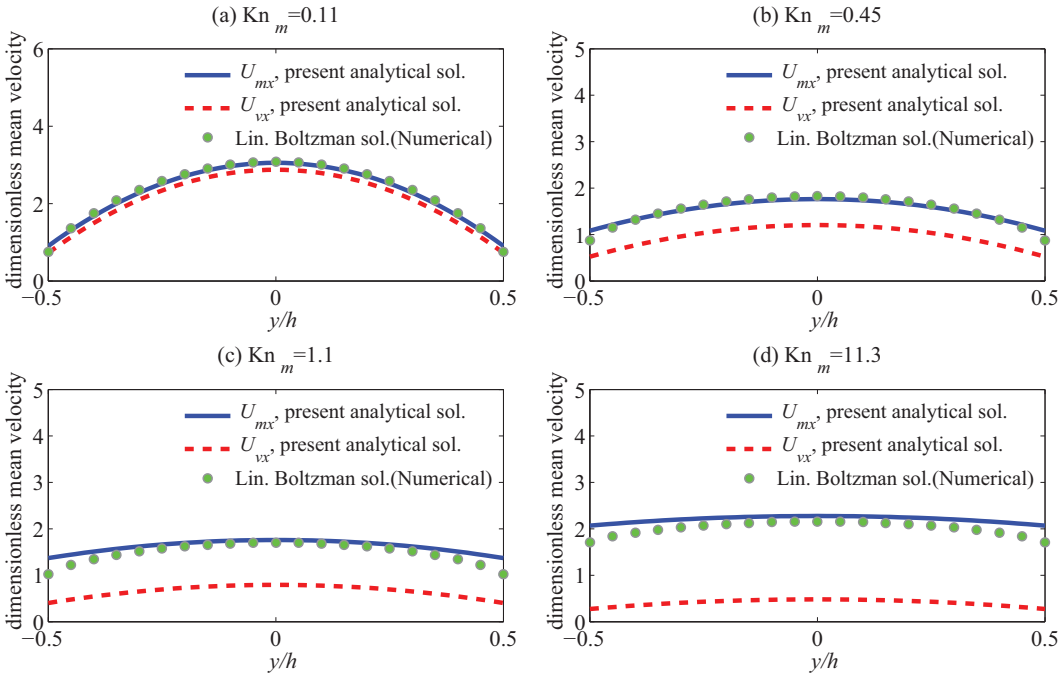

FIG. 8. (Color online) Mass velocity and volume velocity profiles in a microchannel compared with the numerical solution of the linearized Boltzmann equation [4]. U_{mx} and U_{vx} are calculated by Eqs. (26) and (27), respectively. The comparison results are also satisfactory. In addition, for the present model, we can also conclude that (i) the mass velocity and volume velocity are the same in the incompressible flow (Kn $\ll$ 1), (ii) the mass velocity minimum occurs around the Knudsen number of 1; and (iii) the volume velocity decreases continually along with the increasing Kn.

back moderately, whereas the volume velocity continues to decrease.

V. CONCLUSION

Analytical solutions covering a wide range of Knudsen numbers for rarefied gas flow in a microchannel play important roles in many fields. In this paper, we have made an attempt to improve the predictive ability of the analytical solution to this problem. To conclude our work, we present the following three points.

(1) In volume diffusion hydrodynamics, a concept of effective volume diffusion is indispensable for compressible microfluids. Without it, the fluid velocity will become unrealistically high in high-Knudsen-number flow.

(2) A mass flow rate expression for gaseous microchannels is derived, which shows a good agreement with experimental data to a Knudsen number of 50.

(3) For effective volume diffusion hydrodynamics, the Knudsen minimum is concerned only with the mass velocity; the volume velocity does not have an apparent Knudsen minimum.

ACKNOWLEDGMENTS

We are grateful to Professor I. A. Graur for providing the experimental data. This work was financially supported by the National Natural Science Foundation of China (Grant No. 51009079) and National Basic Research Program of China (Grant No. 2011CB013500).

[1] J. C. Maxwell, Phil. Trans. R. Soc. London **170**, 231 (1879).
[2] E. B. Arkilic, M. A. Schmidt, and K. S. Breuer, J. Microelectromech. Syst. **6**, 167 (1997).
[3] G. A. Bird, *Molecular Gas Dynamics and the Direct Simulation of Gas Flows* (Oxford University Press, New York, 1994).
[4] T. Ohwada, Y. Sone, and K. Aoki, Phys. Fluids A **1**, 2042 (1989).
[5] I. A. Graur, J. G. Meolans, and D. E. Zeitoun, Microfluid. Nanofluid. **2**, 64 (2006).
[6] T. Veltzke and J. Thöming, J. Fluid Mech. **698**, 406 (2012).
[7] T. Veltzke, M. Baune, and J. Thöming, Phys. Fluids **24**, 082004 (2012).
[8] Z. Duan, Microfluid. Nanofluid. **12**, 805 (2012).
[9] N. Dongari, A. Agrawal, and A. Agrawal, Int. J. Heat Mass Transfer **50**, 3411 (2007).
[10] N. Dongari and A. Agrawal, Int. J. Heat Mass Transfer **55**, 4352 (2012).
[11] A. Beskok and G. E. Karniadakis, Microscale Thermophys. Eng. **3**, 43 (1999).
[12] G. E. Karniadakis and A. Beskok, *Microflows: Fundamentals and Simulations* (Springer, New York, 2002).
[13] H. Brenner, Int. J. Eng. Sci. **54**, 67 (2012).
[14] S. K. Dadzie and H. Brenner, Phys. Rev. E **86**, 036318 (2012).

[15] T. Ewart, P. Perrier, I. A. Graur, and J. G. Méolans, J. Fluid Mech. **584**, 337 (2007).
[16] H. Brenner, Physica A **349**, 11 (2005).
[17] H. Brenner, Phys. Rev. E **84**, 066317 (2011).
[18] J. Zhang, J. Fan, and F. Fei, Phys. Fluids **22**, 122005 (2010).
[19] V. K. Michalis, A. N. Kalarakis, E. D. Skouras, and V. N. Burganos, Microfluid. Nanofluid. **9**, 847 (2010).
[20] D. A. Lockerby, J. M. Reese, D. R. Emerson, and R. W. Barber, Phys. Rev. E **70**, 017303 (2004).
[21] L. Trilling and H. Y. Wachman, *Rarefied Gas Dynamics: Proceedings of the Sixth International Symposium* (Academic Press, New York, 1969).
[22] L.-S. Luo, Phys. Rev. E **84**, 048301 (2011).
[23] A. B. Huang and R. L. Stoy, Phys. Fluids **9**, 2327 (1966).
[24] S. Takata and H. Funagane, J. Fluid Mech. **669**, 242 (2011).